# The spatial flux of Earth's meteorite falls found via Antarctic data: Supplementary Material

**G.W. Evatt [1], A.R.D. Smedley[1], K.H. Joy[2], L. Hunter[1], W.H. Tey[3], I.D. Abrahams[1,4], and L. Gerrish[5]**

[1]*School of Mathematics, University of Manchester, Manchester, M13 9PL, UK.*

[2]*School of Earth and Environmental Sciences, University of Manchester, Manchester, M13 9PL, UK.*

[3]*Department of Mathematics, Imperial College London, London SW7 2AZ, UK.*

[4]*Isaac Newton Institute for Mathematical Sciences, University of Cambridge, Cambridge, CB3 0EH, UK.*

[5]*British Antarctic Survey, Cambridge, CB3 0ET, UK.*

## S1. ICE FLOW MODEL

There have been several previous attempts in the literature to model the ice flow in the environment of MSZs (Whillans and Cassidy, 1983; Grinsted et al., 2003; Folco et al., 2006). Due to the complex geography often exhibited near MSZs, the poorly determined nature of the bedrock (Zekollari et al., 2019), and uncertainty in basal slip dynamics (Rignot et al., 2011), we avoid carrying out a full 3D modelling of the ice flow and instead consider the surface fluxes of meteorites (see Fig. S1). Here we present a simple and transparent alternative model for the accumulation of meteorites in a blue ice area (BIA; here we use both BIA and MSZ terminology, using BIA when discussing glaciological aspects, and MSZ when meteorites have accumulated on a BIA). This model determines the rate of change in the number of meteorites in a given BIA, by considering the three primary fluxes involved: the rate of direct infalls onto the BIA, the rate of meteorites transported up into the area via ablating ice, and the rate at which meteorites are transported out of the area through surface ice motion (and sometimes wind). Each of these three fluxes needs to be addressed and parameterised.

Taking the surface area of the blue ice to be $B$, and the local fall rate to be $r$, the number of meteorites falling directly on a BIA per unit time is $rB$, (or as a concentration, $r$). The flux of buried meteorites emerging onto the surface is governed by the rate at which the ice ablates (at a water equivalent rate, $\dot{a}$, (Evatt et al., 2016)), and the concentration of meteorites within it. The ablating ice originates from an upstream surface which we define to have an effective surface area, $C_B$, and thus the flux of meteorites falling onto it is given by $rC_B$. We determine $C_B$ by assuming that steady state conditions have been reached. Whilst the residency time of some of the MSZs (Table 1) is not short compared with Holocene timescales, during which ice-flow and climate might reasonably be expected to vary, the presence of stable blue ice areas should still be expected since there is has not been any change in the general location of the mountains that causes the retardation of the ice and resulting blue ice areas. By selecting more productive MSZs, we ensure that we are choosing those that most closely approximate a steady state; by choosing a range of geographically distinct MSZs we aim to mitigate some of these historical and highly localised uncertainties. Furthermore the agreement between equatorial and Antarctic data indicates that this is a reasonable assumption.

Denoting the surface mass balance of the originating surface as $\dot{s}$, then conservation of glacial mass means that this mass gain must equate with the mass loss of blue ice through ablation, or equivalently as volume changes per unit time, namely:

$$B\dot{a} = C_B\dot{s}. \qquad \text{(S1)}$$

Thus we can write the number flux of meteorites, $rC_B$, emerging onto the surface of the BIA as $rB\,\dot{a}/\dot{s}$ (or as a concentration, $r\,\dot{a}/\dot{s}$).

For the flux of meteorites removed from the area, we consider the MSZ geometry and the mean surface ice flow. The surface area of ice leaving the MSZ per unit time is $v_B W$, making the fractional surface area of ice leaving the MSZ per unit time $v_B W/B$, with $v_B$ being the velocity of the ice flow out of the MSZ, $W$ an effective width encapsulating this outward flow, and $B$ is the area of the MSZ. The reduction in meteorite concentration per unit time due to this downstream flow is then $v_B WM/B$, where $M$ is the surface concentration of meteorites.

We do not include a weathering time constant in our model as cold weathering rates are typically 2 to 3 orders of magnitude lower than in hot deserts (as a lower estimate from Bland, 2001, a cold weathering rate of ~5 Myr) and are therefore far longer than the typical surface residency time. Therefore including a weathering constant would have no practical effect on the flux estimates, and in turn our flux estimates rely on ice flow dynamics rather than dating terrestrial ages of individual meteorites. (We note that as our model considers the mean ice flow across each individual stranding zone, it does not preclude instances where localised velocities allow an individual meteorite to reside there for significant periods of time.) Combining the two positive contributions with the ice velocity loss mechanism, the rate of change of meteorite concentration, $\dot{M}$, is given by,

$$\dot{M} = r\left(1+\frac{\dot{a}}{\dot{s}}\right) - \frac{v_B WM}{B}. \qquad (2)$$

The term in brackets can be considered as the ratio of the effective surface area to the physical surface area of the MSZ. This expression can then be solved to give the concentration of meteorites, $M$, within a given blue ice area after an operating time, $t$, (with the concentration zero at time $t = 0$), as follows:

$$M = \frac{rB}{v_B W}\left(1 + \frac{\dot{a}}{\dot{s}}\right)\left(1 - e^{-\frac{v_B W t}{B}}\right). \quad (3)$$

The timescale given by Eqn. (3), $B/v_B W$, is relatively short (see Table 1), and thus we consider a steady state solution where the exponential term → 0. This is equivalent to setting $\dot{M} = 0$ in Eqn. (2). By rearranging, the extra-terrestrial flux can be then predicted accordingly:

$$r = \frac{M v_B W}{B\left(1 + \frac{\dot{a}}{\dot{s}}\right)}. \quad (4)$$

Thus the extra-terrestrial flux rate to Earth can be estimated from the concentrations of meteorites found within a BIA, three glaciological parameters (the ablation rate, the surface mass balance in the effective catchment area, and the mean ice velocity) and appropriate geometric parameters (its area and width). For a given BIA acting as a meteorite stranding zone, our data sources for these variables are as follows. The meteorite collection data for Antarctica (number of finds, mass of finds, location) is taken from the Meteoritical Society's Meteoritical Bulletin Database (MetBull, 2018). (For the sub-divided Allan Hills, Elephant Moraine and Sør Rondane MSZs, finds with nominal locations are reallocated in proportion to the number of finds allocated to each subdivision.) Areas of MSZs are calculated using ArcGIS and BIA boundary features (Hui et al., 2014). For surface mass balance estimates we use gridded annual means from the RACMO regional atmospheric climate model (v. 2.3p1), adjusted in line with their noted elevation dependent (model – in situ) biases (van Wessem et al, 2014a), and averaged over an upstream catchment area.

In situ ablation estimates are sparser and BIAs often exist at a scale less than is resolvable by such regional models. To bridge this gap and construct homogenised ablation estimates that are applicable across the continent we use the semi-empirical psychrometric formula (WMO, 2014), and the standard barometric formula to calculate estimates of the wet-bulb temperature from annual mean dry-bulb temperature estimates and a BIA's altitude. The altitude data is the areal mean BEDMAP2 surface elevation (Fretwell et al., 2013), and temperatures are 2 m modelled estimates (van Wessem et al., 2014b). Next we carry out a least squares regression between in situ ablation measurements and the product of their respective wet-bulb depression (dry-bulb – wet-bulb temperature) and wind speed, following previous studies (Budd et al., 1966), with wind speed estimates from the RACMO model (van Wessem et al., 2014b). In this way we derive an expression for the ablation rate of BIAs given only modelled or easily measured parameters. The locations used in this regression are given in Table S1, whilst the best fit to the data shown in Fig. S2 is given by:

$$\dot{a} = 4.67 V_{10} \Delta_{60} - 4.49, \qquad (5)$$

where $\dot{a}$ is the annual rate of ablation in cm yr$^{-1}$, $V_{10}$ is the 10 m mean annual wind speed, and $\Delta_{60}$ is the wet-bulb depression at a relative humidity of 60%.

The final inputs to our expression for the flux to Earth are $v_B$ the velocity of the ice flow out of the MSZ, and $W$ the effective width, which we calculate in tandem. Here there are two points that need to be addressed. First due to the complex and sinuous nature of the strict BIA boundaries, there is potential for elevated meteorite concentrations to exit one part of a BIA and re-emerge in another; likewise a similar process may occur for proximate BIAs. Both of these processes would lead to biased estimates of the flux. In simpler terms our model accounts for the potential reburial and re-emergence from more than one BIA. Accordingly we construct a convex hull around the BIA boundaries (Hui et al., 2014), calculating the perpendicular component of the ice velocity at this convex hull boundary (Fig. S3). We then use as our estimate for $v_B$ the mean of those perpendicular velocity components that relate to loss from the BIA; for $W$ we use the length of the convex hull that is lossy, scaled according to the ratio of actual BIA area and its convex hull area. For dependent groups of BIAs, each area is attributed the same value of $v_B$, whilst the total lossy perimeter length is again scaled according to its area. In short we seek to calculate the fractional surface area of ice leaving the region. The velocity data that underlies this part of the analysis is the 450 m resolution MEaSUREs Antarctica Ice Velocity dataset (Rignot et al., 2011; Mouginot et al., 2012; Rignot et al., 2017). The uncertainties associated with each pixel's velocity measurement are typically of the same order as the measurement, but for each convex hull we average over ~300 boundary pixels, thus reducing the typical uncertainty to ~0.25 m yr $^{-1}$. Further by taking the mean over geographically separate BIAs, any local velocity measurement bias will be reduced. Whilst our convex hull method accounts for the issue of re-emergence and represents the mean loss from the BIA as a whole (rather than any localised stagnation points), there is potential for it to produce mean boundary velocities that are biased on the high side (for example at Sør Rondane, see Table 1).

By following this methodology for each meteorite bearing BIA where the geographic area is known, we can estimate the local flux to Earth. However individual BIAs may not have been thoroughly searched, or alternatively a small BIA may have been subject to one or two chance direct infalls due to the stochastic nature of meteorite delivery itself — these two cases resulting in outliers either side of the true flux. In total there are 45 identifiable MSZs in the Meteoritical Bulletin Database (12) with > 10 finds, if the principal ice fields of Allan Hills (ALH), Elephant Moraine (EET) and Asuka / Sør Rondane (A) are counted separately. Taken together the flux to Earth estimates from the full set of sites form a lognormal distribution: the distribution of $\log(r)$ values passes both a Kolmogorov-Smirnov test for normality (Massey, 1951) and an Anderson-Darling test (Anderson and Darling, 1952). However, to reduce the effect of the aforementioned biases we restrict further analysis to 13 systematically-searched areas with well-defined spatial extents and more than > 100 meteorite finds (see Table 1). In line with the lognormal nature of the distribution, we calculate our central estimate of the Antarctic flux to Earth as:

$$\bar{r} = 10^{\overline{\log(r)}}, \quad (6)$$

with the ±1 standard error limits calculated in a similar fashion. By excluding finds below a particular mass, we can construct a number-flux spectrum, showing the number of finds above a certain threshold mass. We choose a geometrically spaced set of threshold masses from 0.0625 g to 16.384 kg to sample across the mass range in a logarithmic sense.

Of course there are uncertainties surrounding the single-point glaciological parameters our model has used. These underlying uncertainties, and their interdependencies, are hard to accurately quantify over the long timescales involved, especially locally for small complex areas such as MSZs. However, the time-averaged nature of our model reduces the impact of such variances, as does the combination of data from MSZs that are spatially distributed across Antarctica. To gauge the sensitivity of our model to our single-point glaciological estimates, we conduct a robustness check by allowing the catchment areas of all the MSZs to simultaneously vary by ±25% (i.e. assuming the long-term ratios of ablation to surface mass balance are 25% larger or smaller than present day estimates). In so doing, we find the equatorial fall flux to be 38.1 km$^{-2}$ Myr$^{-1}$ with a pairing factor of 2.50 for the +25% case, and 37.2 km$^{-2}$ Myr$^{-1}$ with a pairing factor of 4.40 for the –25% case. Both of these results are still comfortably lie within the range of the aforementioned studies and literature estimates of the effective pairing factor. This consistency with previous estimates of pairing and flux, each in turn assessed independently, lends additional weight to our approach to calculating the flux and its error through single-point glaciological estimates.

**S2. PAIRING**

The analysis described so far allows us to determine an estimate for the number flux of meteorite fragments, or ‘finds’, but does not address for the ‘pairing issue’ – how many fragments each meteorite fall produces on average. To account for this, there are two possible approaches: to take pairing factors from the literature (Zolensky et al., 2006), or to determine it from a best fit procedure. For the best fit option, we produce a piecewise linear fit for the combined literature datasets (Halliday et al., 1996; Bland et al., 1996a), weighting each by the square root of the number of contributing meteorites. For Bland et al. we take N = 192, scaling from the count at 10 g, and for Halliday et al. N = 62, and breakpoints are specified at 0.1 g, 10 g, 100 g, 1 kg and 10 kg. The combined literature fit is then interpolated onto the same grid spacing as we use for the Antarctic data in order to calculate the r.m.s.e. for a particular assumed pairing value. (For a pairing value $p$, the number flux is reduced as $r' = r/p$, whilst the mass threshold increases as $m' = mp$.) We find a best fit over the mass range of 10 g to 1 kg when $p$ = 3.180.

Note that in general values attributed to these datasets (Halliday et al., 1996; Bland et al., 1996a) are taken from our reanalysis of digitised data provided in a later paper (Bland and Artemieva, 2006). When considering the datasets singly interpolation is carried out on a point-by-point basis, and when considered together weighted fits are used.

In additional to the literature fit, we construct an Antarctic only fit and a combined fit based on the three datasets, but weighted according to the square root of their respective contributing number of meteorites (for Antarctica, we have $N$ = 4,144 when $p$ = 3.180).

With reference to Fig. 3, for comparison we also show previous estimates from the literature (Millard, 1963; Halliday et al, 1984; Halliday et al., 1989; Huss, 1990; Bland et al., 1996a; Bland et al., 1996b;), in all cases unadjusted for latitude.

Antarctic only fit:

$$\log r = -0.048 \log m + 1.739 \qquad 0.1\text{ g} < m < 10\text{ g} \qquad (7)$$

$$\log r = -0.369 \log m + 1.098 \qquad 10\text{ g} < m < 100\text{ g} \qquad (8)$$

$$\log r = -0.703 \log m + 0.764 \qquad 100\text{ g} < m < 1\text{ kg} \qquad (9)$$

$$\log r = -1.057 \log m + 0.764 \qquad 1\text{ kg} < m < 10\text{ kg} \qquad (10)$$

## S3. CALCULATION OF TOTAL RECOVERABLE MASS FLUX

In addition to estimates for the number flux, it is instructive to calculate the total recoverable mass flux. However, distributions with slopes shallower than –1.0 have their mass concentrated in a few large falls and are not sensibly bounded. That is, integrating the mass between zero and an infinite upper bound, does not result in a finite flux rate. Following a previous methodology (Huss, 1990) we instead set a lower mass limit equal to the smallest meteorite found, and an upper mass limit that would correspond to a single fall event, and integrate between these limits to find the total recoverable mass flux. We consider the results from our comparative studies (Halliday et a;., 1996; Bland et al., 1996a) together, taking the lower mass limit as the smallest mass plotted by Bland and Artemieva (2006), whilst the fit relies on a total of 254 meteorite falls.

## S4. LATITUDINAL MODEL

It is not obvious what effect latitude will have on the frequency of falls for a particular planet. To see why, first note that the majority of asteroid-derived material which will strike a planet will have had an overlapping orbit and shared a near-common plane (taken together, we crudely refer to these combined orbits as the 'fall annulus'). This is not to say that initially inclined material cannot strike the planet. But rather that the probability of them ever being in the same place at the same time is so small that, in comparison to material with low orbital inclinations, their contribution to the total frequency is negligible (Halliday, 1964; Le Feuvre and Wieczorek, 2008). This geometric reasoning immediately highlights that material does not, at least initially, approach the planet uniformly from all directions. We also note that the following arguments are independent of the meteorite composition (density, material, etc.).

To continue: we can expect that the size and density of a planet (i.e. its gravitational attraction), and the speed of the incoming asteroids will have an effect on the fall distribution with latitude. That is, small planets will deflect the orbit of an asteroid less than a large planet, and hence lead to a lower frequency of falls nearer the ecliptic poles. Similarly, fast moving material might overshoot the planet entirely, thereby reducing the fall frequency at the ecliptic poles, whereas slow moving material will give a larger contribution. Likewise the axial tilt of the planet will have a significant effect, for the tilt determines the degree to which a given latitude band can receive two contributions: from head-on falls and, for certain latitudes, from overshoot (where the material passes the planet's pole to land on the side facing away from the initial trajectory). Thus, a robust and transparent method for quantifying the resulting latitudinal dependence is required.

To calculate the fall flux dependence upon latitude, we model the Earth as a sphere, with centre **O**, which is bombarded by material from the fall annulus (Fig. S4). Incoming material starts from the outermost part of the fall annulus, and this material is modelled to have formed part of an 'asteroid plane' that is perpendicular to the ecliptic. The axis between point **O** and the centre of the asteroid plane, point **A**, is the radiant for that particular asteroid plane. Indeed, the outermost part of the fall annulus is composed of a complete rotation (about **O**) of asteroid planes; this rotation of asteroid planes reflects the fact that although the material is initially following Earth-independent orbits, only those asteroids initially directed towards the Earth will fall under its gravitational influence. We need give attention to the contribution of material to Earth from just one of these asteroid planes to understand the key underlying physics and geometry.

Each object within the asteroid plane starts far enough away from Earth that its potential energy is negligible, and with an initial velocity $V_0$ directed parallel to the radiant **OA**. Denoting the object's starting point as **C**, we term the angle between **AC** and **AD** as $\eta$, and term the distance between **A** and **C** as $\sigma$; thus the object's initial angular momentum (with respect to an Earth orbit) is $mV_0\sigma$, and its total energy is the same as its initial kinetic energy, $mV_0^2/2$, where $m$ is the mass of the object.

With this information one can write the well-known Orbit Equation, which governs an object's orbit under the influence of the Earth (i.e. where the Sun's tidal forces have become negligible in comparison to the Earth's), as:

$$\frac{1}{r} = \frac{1}{\sigma}\sin\theta + \frac{GM_E}{V_0^2\sigma^2}(1-\cos\theta). \qquad (11)$$

Here $M_E$ is the mass of the Earth, $G$ the gravitational constant, $r$ the radial distance from the centre of the Earth to the object, and $\theta$ is the angle between the radiant and a straight line to the object. We shall shortly see that it is useful to rearrange Eqn. (11) to obtain $\sigma$ in terms of $\theta$ when the object reaches the Earth's surface, $r = R$, namely:

$$\sigma = \frac{R}{2}\sin\theta + \sqrt{\left((R\sin\theta)^2 + \frac{4GM_E R}{V_0^2}(1-\cos\theta)\right)}. \quad (12)$$

We next calculate the area of the asteroid plane that can contribute meteorites to a given area of Earth, and how that asteroidal area varies as Earth's longitude and latitude varies. We commence by assuming that the Earth's polar axis is perpendicular to the ecliptic, and adjust for this axial tilt later. This enables us to add all of the asteroidal areas for a given latitude band, and then compare the totals in order to observe any latitudinal variation. To achieve this we make small variations in both $\theta$ and $\eta$ ($d\theta$ and $d\eta$; see Fig. S4) to relate the respective incremental areas on the Earth's surface and on the asteroid plane:

$$A_E = R\sin\theta\, d\eta\, R\, d\theta, \quad (13)$$

$$A_P = \sigma\, d\eta\, d\sigma. \quad (14)$$

The ratio $A_P/A_E$ then acts as a scaling factor between the asteroid plane and the Earth's surface. This means that if objects are coming from that portion of the asteroid plane at a rate $\varphi$ per unit area per unit time, then the rate of objects reaching the corresponding area of Earth is $\varphi\, A_P/A_E$ per unit area per unit time. And so for a given angle of latitude, $\theta_l$, and angle of longitude, $\psi$, the fall frequency, $df$, for that incremental area is thus:

$$df(\theta_l,\psi) = \varphi \frac{A_P}{A_E} R^2\, d\psi \sin\theta_l d\theta_l. \quad (15)$$

Making use of Eqns. (13) and (14), we convert Eqn. (15) into:

$$df(\theta_l,\psi) = \varphi\, \sigma \frac{\sin\theta_l}{\sin\theta} \frac{d\sigma\, d\theta_l\, d\psi}{d\theta}. \quad (16)$$

To simplify matters one can show from geometrical means that the three angles present in Eqn. (16), $\theta$, $\theta_l$, and $\psi$, are linked via the relation:

$$\cos\theta = \cos\theta_l \cos\psi, \quad (17)$$

and thus the total fall frequency, $f$, of material from the asteroid plane landing in a given latitude band is obtained by integrating Eqn. (16), along with the constraint of Eqn. (17), across all longitudinal values, $\psi$, making sure to take only positive contributions (negative values correspond to falls which have already hit the Earth but whose mathematical trajectories continue onwards within the Earth to strike the surface again). However it is the normalised fall frequency, $F_e$, which is more useful for our purposes, and this can be written as:

$$F_e(\theta_l) = \left\| \int_{-\pi}^{\pi} \left[\frac{\sigma}{\sin\theta}\frac{d\sigma}{d\theta}\right]^{+} d\psi \right\|. \quad (18)$$

Here ||.|| denotes the normalisation of the integral inside with respect to the maximum value it takes across the range of latitudes (hence terms involving the constants $\varphi$, $R$ and $dl = \sin\theta_l \, d\theta_l$ which appeared in Eqn. (16) are not present in Eqn. (18)), and [.]+ denotes the consideration of only positive values.

As written, Eqn. (18) only represents the contribution to a given latitude band from a single one of the asteroid planes which surround the Earth (Fig. S4). That said, when the tilt of the polar axis of the Earth is not considered, then symmetry means one does not need to consider this second rotation, and thus Eqn. (18) is all one needs to use to calculate the normalised fall frequency as a function of ecliptic latitude.

To capture the effect of the tilt of the Earth's rotation axis, we need to consider two further rotations of the coordinate frame shown in Fig. S4: the first for the tilt of the Earth, $\tau$, towards the asteroid plane (which for Earth we take as 23.4°), and the second is a rotation of the asteroid plane (equivalent to a rotation of the Earth about the ecliptic pole), by an amount $\alpha$. It is this second rotation of the asteroid planes that we must also integrate over all angles of longitude. The net result is a straightforward modification to Eqn. (18), where the geographic fall frequency, $F$, for a particular latitude is now given by the double integral:

$$F(\theta_l) = \left\| \int_{-\pi}^{\pi} \int_{-\pi}^{\pi} \left[ \frac{\sigma}{\sin\theta} \frac{d\sigma}{d\theta} \right]^{+} d\psi \, d\alpha \right\|, \quad (19)$$

where we now have the geometric relation (via the two axial rotations),

$$\cos\theta = \cos\tau \cos\alpha \cos\theta_l \cos\psi - \sin\alpha \cos\theta_l \sin\psi + \sin\tau \cos\alpha \sin\theta_l, \quad (20)$$

and $\sigma$ is still given by Eqn. (12).

The evaluation of Eqn. (19) produces normalised fall frequencies, for any planet of radius $R$, mass $M_E$, tilt $\tau$, and with the falls having initial velocity from the asteroid plane $V_0$. Given that observed falls have a distribution of entry velocities, one can take an appropriate weighted average of Eqn. (19) over the initial velocities. By conservation of energy, the link between the entry velocity (at altitude $h$), $V_1$, and initial velocity, $V_0$, is given by:

$$\frac{mV_1^2}{2} - \frac{M_E G}{(R+h)} = \frac{mV_0^2}{2}. \quad (21)$$

We achieve this by using an observed velocity distribution of witnessed fireballs (NASA CNEOS, 2018) (where by definition the air resistance has had an appreciable effect), and then scale it upwards so that the mean matches an estimate of high altitude characteristic velocities (Moorhead, 2018), which is approximately 20 km s$^{-1}$ (we also confirm that the lowest velocities do indeed surpass the Earth's escape velocity of ~11.3 km s$^{-1}$). A sensitivity analysis found no sizeable deviation between the results using the full velocity distribution and the results using only the mean of the distribution (20 km s$^{-1}$; the pole to equator ratio being 58%). We also found that ±10% velocity changes from the 20 km s$^{-1}$ estimate made only minor changes to the results: a ratio of 65% for the 17.5 km s$^{-1}$ case, and a ratio of 55% for the 22.5 km s$^{-1}$ case. Changes of ± 25% did not alter the overall trend of a decreasing fall frequency with latitude, but the magnitude of the fall frequency did appreciably alter for the slower velocities; for example, a ratio of 78%

for the 15 km $s^{-1}$ case, and a ratio of 52% ratio for the 25 km $s^{-1}$ case. We also found that as velocities increased further, then the polar ratio tends to an asymptotic value of around 41%.

We can now account for the latitudinal variation in observed fluxes of meteorites, and, by dividing by the value of the latitudinal curve shown in Fig. 2 for the mean latitude of the finds, calculate an equatorial-equivalent value. For Antarctic finds from high-quality MSZs (mean latitude of 77.48°) the value is 0.666. For the two key surface datasets in a similar mass range as the Antarctic data, the equivalent value for the three desert sites study (Bland et al., 1996a) (mean latitude 30.94°) is 0.918, and for the Canadian camera network study (Halliday et al., 1996) (nominal latitude 52°) is 0.793.

To convert from equatorial-equivalent fluxes to whole earth fluxes, requires, in addition to multiplication by the surface area of the earth, multiplication by the area-weighted mean of the latitude curve. This takes the value 0.890.

Finally, we acknowledge the fact that some of these results appear to have been calculated before (Halliday, 1964). However, only minimal wording and no working was offered in that paper as to the methodology used. This means we cannot say for sure whether our method presented here was the same as that employed over 50 years ago. However, where results were presented in that study, our model produces extremely similar results to all of them. What we can say for certain, is that our presented methodology allows for results to be objectivity calculated using the full range of velocities, tilts, sizes and masses, and any corresponding distributions thereof.

## S5. FIREBALL STATISTICAL ANALYSIS

Fireball data was retrieved from the CNEOS (NASA Center for Near Earth Objects) database (NASA CNEOS, 2018) and consisted of 566 fireballs that had latitude entries recorded over the period of 1988 to 2018. We consider both Earth's hemispheres together (from the symmetry of the underlying physics and relative geometries of the Earth, ecliptic plane and asteroid belt) and bin the data into 11 latitude bands (Sturges, 1926; Shimazaki and Shinomoto, 2007) between 0° and 90°. For each latitude band we calculate the normalised impact frequency (number of fireballs observed per $km^2$, scaled). We rely on the CNEOS reported latitude of peak brightness and do not attempt to adjust for any atmospheric effect due to retardation; we calculate that the uncertainty associated with this simplification is < 1º which is much less than the bin width (the mean absolute deviation of peak brightness vs ground latitude = 0.29º, its 95th percentile = 0.97º). We make no use of the fireball mass, and only analyse their locations to determine the latitudinal dependence of flux. Our latitude expression is normalised at a latitude of 0°, and the observed normalised impact frequency, the uniform case, and results from a previous study (Le Feuvre and Wieczorek, 2008) are all scaled so they have a common mean and are comparable.

Visually, our expression for the latitude variation appears to fit the observations far better than the assumption of a uniform distribution, or indeed that presented by earlier authors (Le Feuvre and Wieczorek, 2008). To put this on a quantitative basis we apply an F-test, finding that our latitudinal model is significantly better than assuming a uniform frequency at the 95% confidence level ($p = 0.012$). In addition we carry out a bootstrap analysis drawing $10^5$ random samples from a uniform distribution, each with 566 members, to calculate the root mean square error, the mean absolute distribution, and the slope of the best fit regression for each. This test allows us to estimate the overall probability that a uniform distribution produces values at least as great as those observed as $p = 0.016 \pm 0.007$. Repeating this process by drawing random samples from a Le Feuvre–Wieczorek-based distribution gives $p = 0.033 \pm 0.013$, and we thus conclude that at the 95% level our description of the latitude variation fits the fireball observations better than both these alternate distributions. However, we cannot rule out latitudinal, other biases, or collection efficiencies, particularly during the early years of observation when the satellite coverage was incomplete (Brown et al., 2002), issues which may relate to the outlier in the second bin. Accordingly, we repeat the analysis for the last 10 years, but still find that at the 95% level our latitudinal variation explains the observations better than a uniform distribution.

## REFERENCES CITED IN SUPPLEMENTARY MATERIAL ONLY


Anderson, T.W., and Darling, D.A., 1952, Asymptotic Theory of Certain "Goodness of Fit" Criteria Based on Stochastic Processes: The Annals of Mathematical Statistics, v. 23, p. 193–212, http://www.jstor.org/stable/2236446.

Bintanja, R., 1999, On the glaciological, meteorological, and climatological significance of Antarctic blue ice areas: Rev. Geophys., v. 37, p. 337–359, doi:10.1029/1999RG900007.

Bland, P.A., Berry, F.J., Smith, T.B., Skinner, S.J., and Pillinger, C.T., 1996b, The flux of meteorites to the earth and weathering in hot desert ordinary chondrite finds: Geochimica et Cosmochimica Acta, v. 60, p. 2053–2059, doi:10.1016/0016-7037(96)00125-1.

Bland, P., 2001, Quantification of meteorite infall rates from accumulations in deserts, and meteorite accumulations on Mars, in Peucker-Ehrenbrink, B., and Schmitz, B., eds., Accretion of extraterrestrial matter throughout Earth’s history: New York, Kluwer Academic/Plenum, p. 267–298.

Budd, W., 1966, Ablation from an Antarctic Ice Surface, in Conference on Physics of Snow and Ice, Sapporo, Japan, p. 431–446.

Clow, G.D., McKay, C.P., Simmons, G.M., and Wharton, R.A., 1988, Climatological observations and predicted sublimation rates at Lake Hoare, Antarctica.: Journal of climate, v. 1, p. 715–728.

Faure, G., and Buchanan, D., 1991, Ablation Rates of the Ice Fields in the Vicinity of the Allan Hills, Victoria Land, Antarctica: Contributions to Antarctic Research II, v. 53, p. 19–31.

Folco, L., Welten, K.C., Jull, A.J.T., Nishiizumi, K., and Zeoli, A., 2006, Meteorites constrain the age of Antarctic ice at the Frontier Mountain blue ice field (northern Victoria Land): Earth and Planetary Science Letters, v. 248, p. 209–216, doi:10.1016/j.epsl.2006.05.022.

Fretwell, P. et al., 2013, Bedmap2: Improved ice bed, surface and thickness datasets for Antarctica: Cryosphere, v. 7, p. 375–393, doi:10.5194/tc-7-375-2013.

Grinsted, A., Moore, J., Spikes, V.B., and Sinisalo, A., 2003, Dating Antarctic blue ice areas using a novel ice flow model: Geophysical Research Letters, v. 30, p. 2005, doi:10.1029/2003GL017957.

Halliday, I., Blackwell, A.T., and Griffin, A.A., 1984, The Frequency of Meteorite Falls on the Earth: Science, v. 223, p. 1405 LP – 1407, doi:10.1126/science.223.4643.1405.

Halliday, I., Blackwell, A.T., and Griffin, A.A., 1989, The flux of meteorites on the Earth’s surface: Meteoritics, v. 24, p. 173–178, doi:10.1111/j.1945-5100.1989.tb00959.x.

Hui, F. et al., 2014, Mapping blue-ice areas in Antarctica using ETM+ and MODIS data: Annals of Glaciology, v. 55, p. 129–137, doi:10.3189/2014AoG66A069.

Massey Jr, F.J., 1951, The Kolmogorov-Smirnov test for goodness of fit: Journal of the American Statistical Association, v. 46, p. 68–78, doi:10.1080/01621459.1951.10500769.

Millard, H.T., 1963, The Rate of Arrival of Meteorites at the Surface of the Earth: Journal of Geophysical Research, v. 68, p. 4297–4303, doi:10.1029/JZ068i014p04297.

Moorhead, A. V, 2018, Deconvoluting measurement uncertainty from the meteor speed distribution: Meteoritics & Planetary Science, v. 53, p. 1292–1298, doi:10.1111/maps.13066.

Mouginot, J., Scheuch, B., and Rignot, E., 2012, Mapping of ice motion in antarctica using synthetic-aperture radar data: Remote Sensing, v. 4, p. 2753–2767, doi:10.3390/rs4092753.

Nagata, T., 1978, A possible mechanism of the concentration of meteorites within the Meteorite Ice Field in Antarctica: Mem. Natl. Inst. Polar Res. Spec. Issue Jpn, v. 8, p. 70–92.

Rignot, E., Mouginot, J., and Scheuchl, B., 2011, Ice Flow of the Antarctic Ice Sheet: Science, v. 333, p. 1427–1430, doi:10.1126/science.1208336.

Rignot, E., Mouginot, J., Scheuchl, B., 2017, MEaSUREs InSAR-Based Antarctica Ice Velocity Map, Version 2: NASA National Snow and Ice Data Center Distributed Active Archive Center, Boulder, Colorado, USA (January 2018).

Shimazaki, H., and Shinomoto, S., 2007, A Method for Selecting the Bin Size of a Time Histogram: Neural Computation, v. 19, p. 1503–1527, doi:10.1162/neco.2007.19.6.1503.

Stearns, C.R., and Weidner, G.A., 1993, Sensible and latent heat flux estimates in Antarctica, in Bromwich, D.H. and Stearns, C.R. eds., Antarctic Meteorology and Climatology, Studies Based on Automatic Weather Stations, Antarct. Res. Ser., vol. 61, Washington, DC, AGU, p. 109–138.

Sturges, H.A., 1926, The Choice of a Class Interval: Journal of the American Statistical Association, v. 21, p. 65–66, doi:10.1080/01621459.1926.10502161.

Takahashi, S., Naruse, R., Nakawo, M., and Mae, S., 1988, A bare ice field in East Queen Maud Land, Antarctica, caused by horizontal divergence of drifting snow: Ann. Glaciol, v. 11, p. 156–160, doi:10.3189/S0260305500006479.

Takahashi, S., Endoh, T., Azume, N., and Meshida, S., 1992, Bare Ice Fields Developed in the Inland Part of Antarctica, in Proc. NIPR Symp. Polar Meteorol. Glaciol., p. 128–139.

van Wessem, J.M. et al., 2014a, Improved representation of East Antarctic surface mass balance in a regional atmospheric climate model: Journal of Glaciology, v. 60, p. 761–770, doi:10.3189/2014JoG14J051.

van Wessem, J.M., Reijmer, C.H., Lenaerts, J.T.M., Van De Berg, W.J., Van Den Broeke, M.R., and Van Meijgaard, E., 2014b, Updated cloud physics in a regional atmospheric climate model improves the modelled surface energy balance of Antarctica: The Cryosphere, v. 8, p. 125–135, doi:10.5194/tc-8-125-2014.

Vaughan, D., and Russell, J., 1997, Compilation of Surface Mass Balance Measurements in Antarctica, 1997: British Antarctic Survey, Cambridge, UK.

Whillans, I.M., and Cassidy, W.A., 1983, Catch a falling star: Meteorites and old ice: Science, v. 222, p. 55–57, doi:10.1126/science.222.4619.55.

WMO, 2008, World Meteorological Organization No 8: Guide to Meteorological Instruments and Methods of Observation (Seventh Edition).

453 **SUPPLEMENTARY MATERIAL FIGURES AND CAPTIONS**

454

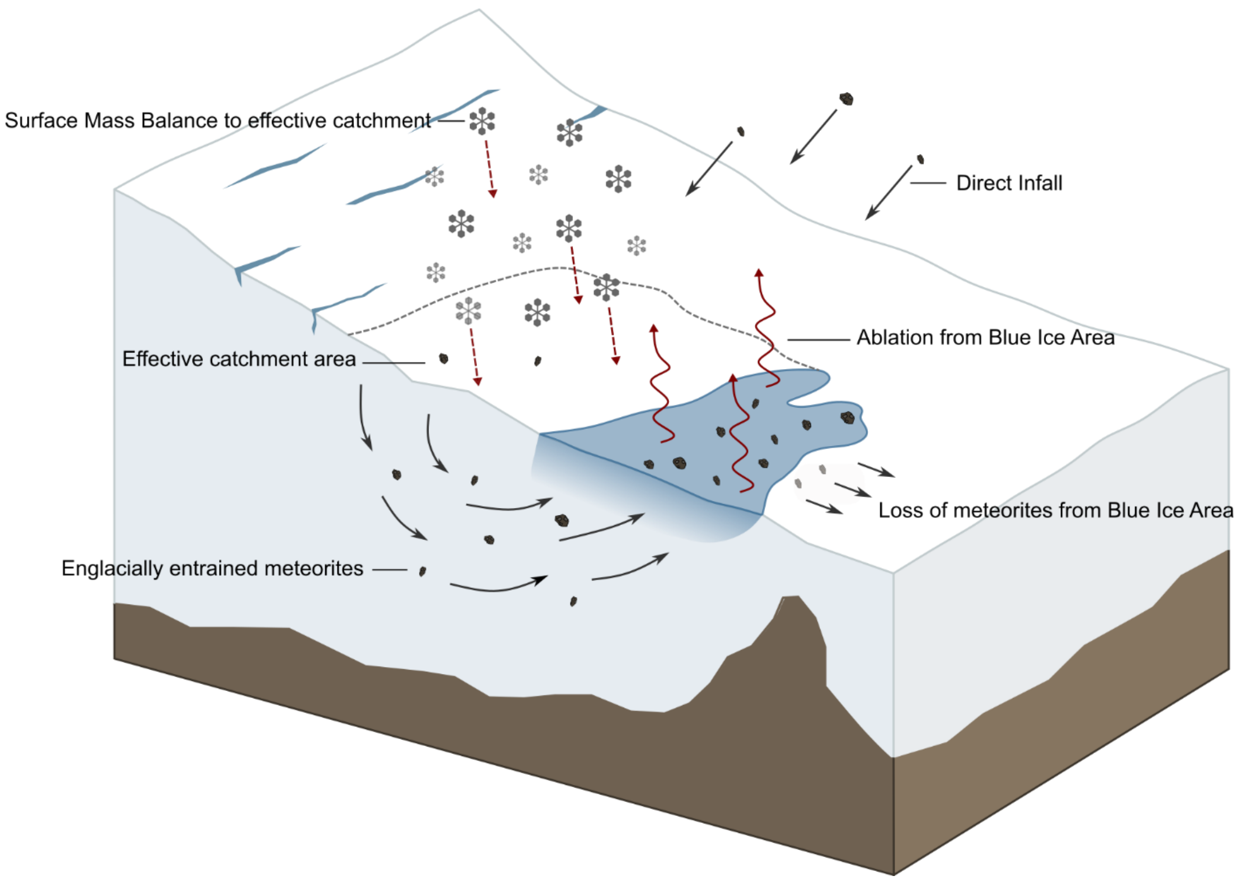


455

456

457 Figure S1. Meteorite stranding zone ice flow and loss schematic.

458

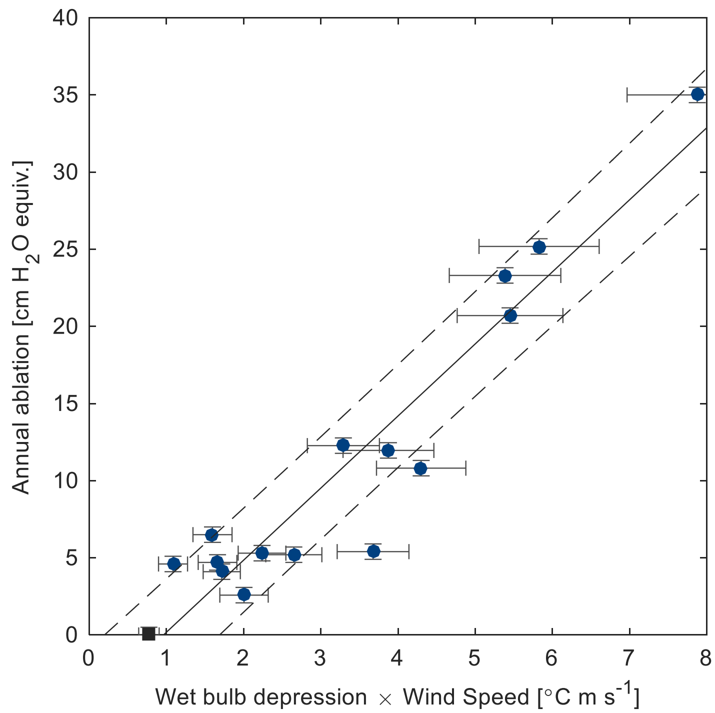


Figure S2. Regression between in situ measurements of annual ablation, $\dot{a}$ [cm yr$^{-1}$ water equivalent] and satellite- and model-derived values of $V_{10}\Delta_{60}$, ($R^2$ = 0.900, r.m.s. of residuals = 3.225). Uncertainty estimates are model-derived r.m.s.d. values (van Wessem et al., 2014b); annual ablation uncertainties are taken to be ±0.5 cm yr$^{-1}$.

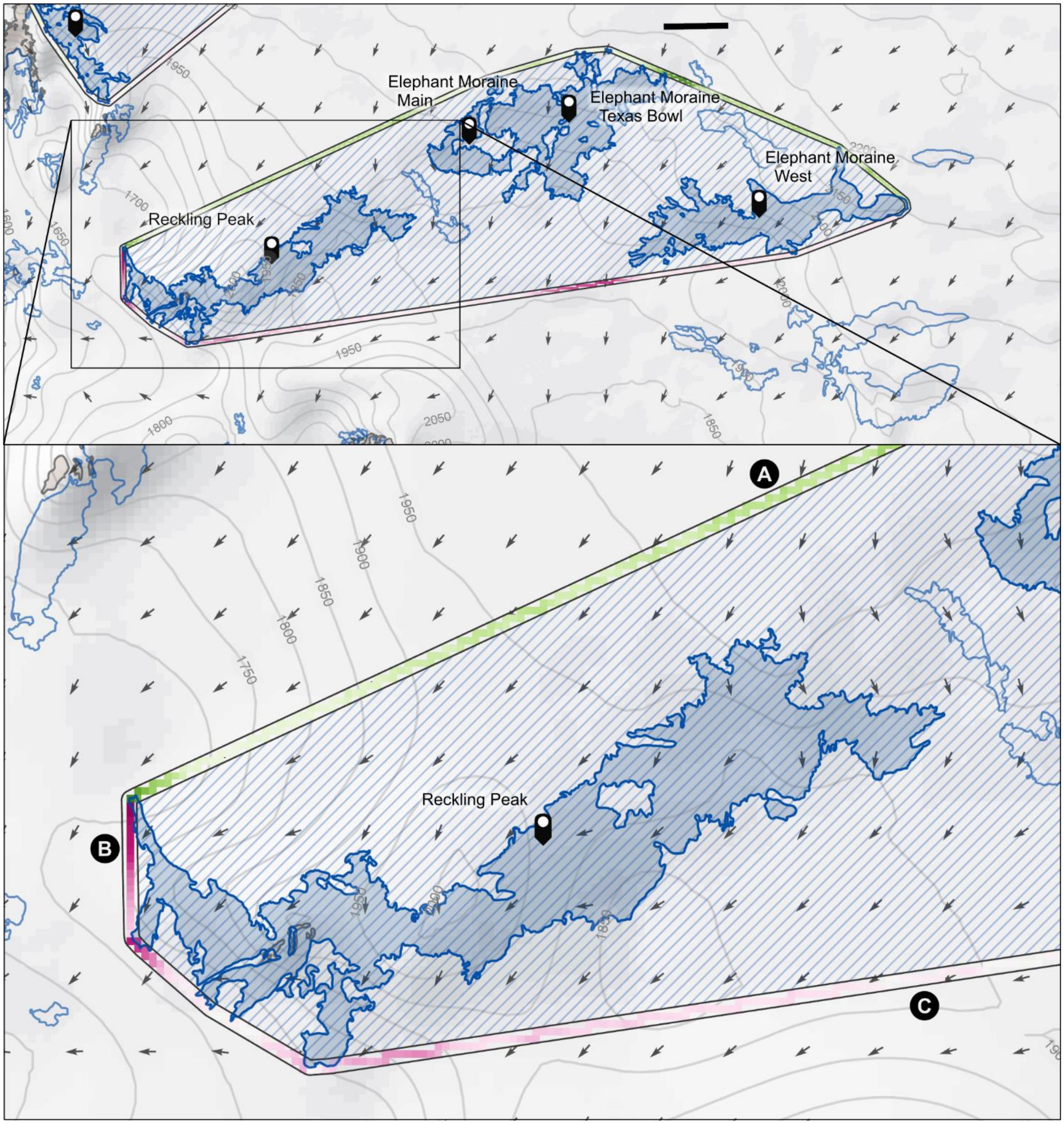


Figure S3. Example convex hull (minimum bounding geometry) for Reckling Peak and Elephant Moraine region used to calculate mean fractional ice surface area loss. Tram lines indicate boundary of convex hull (hatched area) around proximate BIAs. Arrows show ice flow direction. High values of perpendicular boundary flow velocity into BIA are coloured green (A), whilst losses from the region are coloured magenta (B). Less extreme values can result from ice flow parallel to the convex hull boundary (C), or lower ice flow speeds.

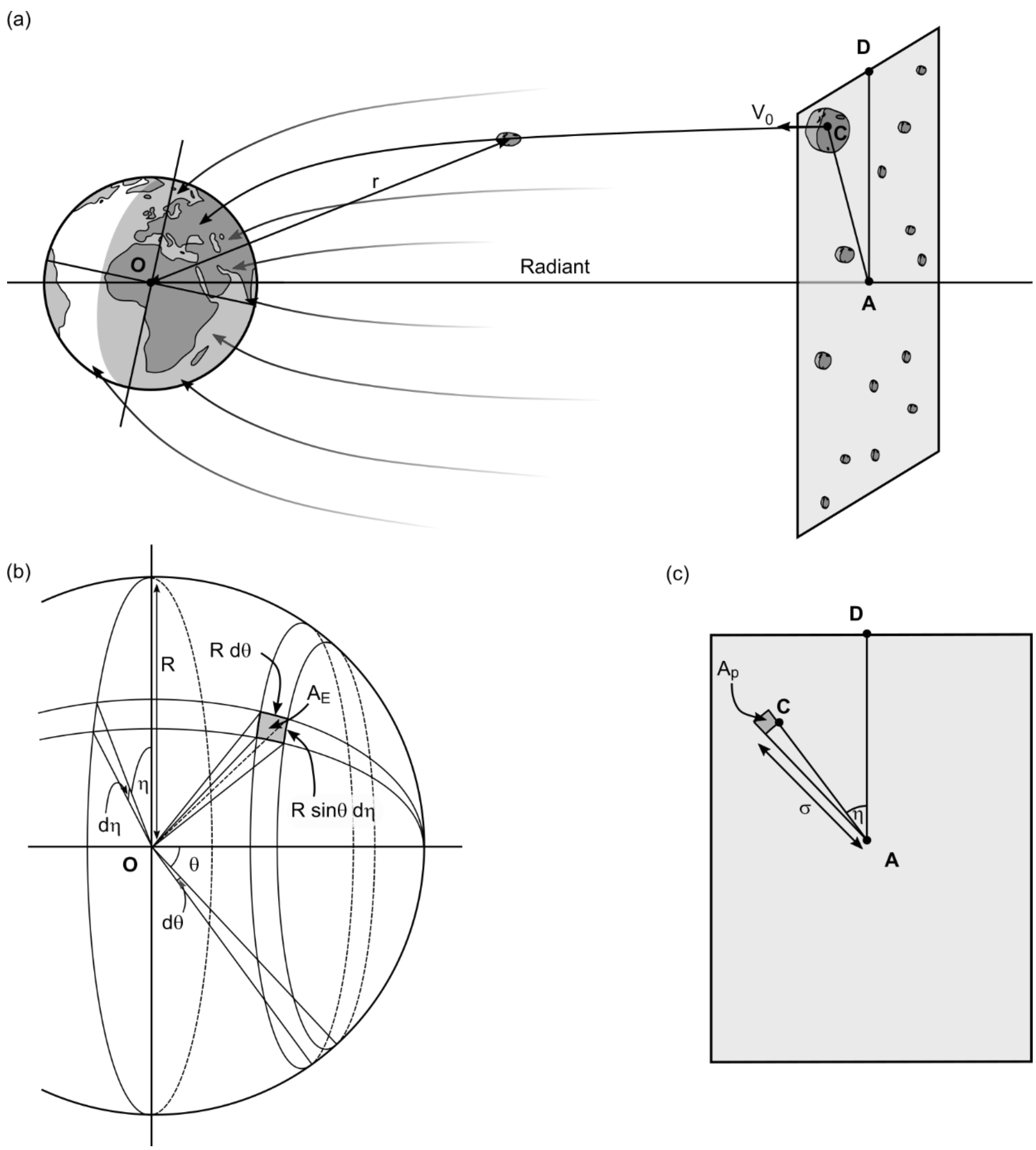


Figure S4. (a) Schematic overview of Earth–asteroid geometry (b) Detail of geometry on Earth's surface showing calculation of $A_E$ (c) End view of asteroid plane geometry and calculation of $A_P$.

Table S1. In situ blue ice ablation measurement sites, data summary, and citation.

| Location name | Geographic coordinates | Nominal altitude (km) | Temperature (2 m, dry-bulb) (°C) | Wind speed (10 m) (m s$^{-1}$) | In situ ablation rate (cm yr$^{-1}$) |
|---|---|---|---|---|---|
| Lake Hoare (Bintanja, 1999; Clow et al., 1988) | 77° 38′S 162° 52′E | 0.03 | –17.7 | 10.08 | 35.00 |
| Mawson Station (nr Mawson) (Budd, 1966; Bintanja, 1999) | 67° 41'S 62° 55'E | 0.29 | –18.2 | 7.51 | 25.18 |
| Reeves Glacier (PAT site) (Bintanja, 1999; 46) | 74° 54' S 163° 06'E | 0.03 | –21.5 | 9.28 | 20.70 |
| Seal Rock, Sør Rondane (Bintanja, 1999, Takahashi et al., 1992) | 71° 31'S 24° 05'E | 0.91 | –20.5 | 7.67 | 23.30 |
| Scharffenberg Botnen, Queen Maud Land (Bintanja, 1999) | 74° 35′S 11° 03′W | 1.41 | –23.0 | 6.31 | 11.96 |
| Mawson Station (nr Mawson, further inland) (Budd, 1966, Bintanja, 1999) | 67° 58'S 62° 26'E | 1.06 | –24.7 | 8.35 | 10.81 |
| Gunnestadbreen, Sør Rondane (Bintanja, 1999) | 72° 03′S 23° 50′E | 1.37 | –27.8 | 7.96 | 12.27 |
| Borg Mass, Queen Maud Land (Bintanja, 1999) | 72° 45′S 03° 30′E | 2.70 | –34.1 | 7.18 | 2.58 |
| Allan Hills Main Icefield (Bintanja, 1999; Faure and Buchanan, 1991) | 76° 41'S 159° 16'E | 2.10 | –35.9 | 10.23 | 5.30 |
| Reckling Moraine (Bintanja, 1999, Faure and Buchanan, 1991) | 76° 15'S 158° 37' E | 1.90 | –36.8 | 8.49 | 4.70 |
| Elephant Moraine Main Icefield (Bintanja, 1999, Faure and Buchanan, 1991) | 76° 19'S 157° 09'E | 2.00 | –39.1 | 10.84 | 4.10 |
| Lewis Cliff Ice Tongue (Vaughan and Russell, 1997) | 84° 21'S 161° 22'E | 2.27 | –38.9 | 6.49 | 4.60 |
| Frontier Mountain (Folco et al., 2002) | 72° 56'S 160° 24'E | 2.14 | –36.1 | 7.40 | 6.50 |
| Mizuho Station (Takahashi et al., 1988) | 70° 42'S 44° 20'E | 2.24 | –33.7 | 9.69 | 5.20 |
| Yamato Mountains (Bintanja, 1999, Nagata, 1978) | 71° 50'S 36° 20'E | 2.31 | –31.8 | 11.22 | 5.40 |
| Minimum | N/A | 3.43 | –44.8 | 7.28 | 0.00 |

*Note*: The data inputs for the location referred to as 'Minimum' are based on the altitude and temperature above which no BIAs form (Hui et al., 2014).